SPACE RESEARCH COORDINATION CENTER

ANALYSIS OF OGO-6 OBSERVATIONS OF THE OI 5577A TROPICAL NIGHTGLOW

BY

R. J. THOMAS AND T. M. DONAHUE

SRCC REPORT NO. 168

UNIVERSITY OF PITTSBURGH

PITTSBURGH, PENNSYLVANIA

APRIL 1972

The Space Research Coordination Center, established in May, 1963, has the following functions: (1) it administers predoctoral and postdoctoral fellowships in space-related science and engineering programs; (2) it makes available, on application and after review, allocations to assist new faculty members in the Division of the Natural Sciences and the School of Engineering to initiate research programs or to permit established faculty members to do preliminary; work on research ideas of a novel character; (3) in the Division of the Natural Sciences it makes an annual allocation of funds to the Interdisciplinary Laboratory for Atmospheric and Space Sciences; (4) in the School of Engineering it makes a similar allocation of funds to the Department of Metallurgical and Materials Engineering and to the program in Engineering Systems Management of the Department of Industrial Engineering; and (5) in concert with the University's Knowledge Availability Systems Center, it seeks to assist in the orderly transfer of new space-generated knowledge in industrial application. The Center also issues periodic reports of space-oriented research and a comprehensive annual report.

The Center is supported by an Institutional Grant (NsG-416) from the National Aeronautics and Space Administration, strongly supplemented by grants from the A. W. Mellon Educational and Charitable Trust, the Maurice Falk Medical Fund, the Richard King Mellon Foundation and the Sarah Mellon Scaife Foundation. Much of the work described in SRCC reports is financed by other grants, made to individual faculty members.

Analysis of OGO-6 Observations of the OI 5577A Tropical Nightglow

R. J. Thomas and T. M. Donahue*

Department of Physics

University of Pittsburgh

Pittsburgh, Pennsylvania 15213

Abstract

Atomic oxygen green line data from the horizon scanning photometer on OGO-6 has been examined. Unfolding the satellite data from the tropical F-region yields altitude and latitude variations of the $O(^1S)$ emissions. The spatial variations of the tropical F-region electron density are then calculated by assuming dissociative recombination and using a model atmosphere. Where comparisons to ground-based data are possible the results are good. Thus, the satellite observations constitute a form of topside sounding of the ionosphere below the F-peak and provide synoptic data about this portion of the ionosphere otherwise impractical to obtain.

---

*Present Address: Harvard University, Cambridge, Mass. 02138

Introduction

Among the twenty-six separate experiments flown on the OGO-6 aeronomy satellite was a horizon scanning photometer devoted to the study of the green and yellow airglow. This photometer has a narrow field of view and good scattered light protection. These properties have allowed it to observe the dayglow as well as twilight and nightglow. Since the photometer was designed to scan in a vertical plane in a large number of small steps, it can make a high spatial resolution study of the narrow thermospheric airglow layers.

Papers devoted to the detailed characteristics of the photometer and to the data pertaining to the "mesospheric" airglow will be published later. The purpose of the present note is to discuss the high altitude (F-region) green emission observed by the instrument only at low latitudes in the nightglow. The OI 5577A line should be excited in the night time ionosphere as a result of the formation of O_2^+ ions in charge transfer reactions between O^+ and O_2 molecules and the subsequent dissociative recombination of the molecular ions. This process was shown long ago to be the source of the tropical enhancement of the oxygen red doublet at 6300A. But the green emission must compete with the much stronger and always present airglow arising near 95 km. Disentangling these separate contributions to the 5577A airglow in observations from the surface is difficult, although Van Zandt and Peterson (1968) have shown that it can be done. Gulledge et al (1968) have observed the F-region green emission directly in a rocket experiment. Viewed almost horizontally from above, the F-region emission clearly stands out as a separate airglow feature. Furthermore, the large optical path associated with slantwise

observation causes an amplification by a factor of about 10-20 in the surface brightness of the F-region airglow. This allows detection of features which in the vertical would contribute only a few Rayleighs to the airglow intensity. For the 95 km airglow, the amplification factor is about 50.

In what follows we shall show that it is possible to take advantage of repeated scans, through the same airglow emission features obtained at successive positions along the satellite orbit, to unfold the local volume emission rates of the green line as a function of altitude. On the assumption that these rates are a reflection of the local rate of conversion of O^+ to O_2^+, it is then possible to deduce the O^+ density if the O_2 density, the rate constant of the reaction

$$O_2^+ + e \rightarrow O(^3P) + O(^1S), \qquad (1)$$

and the rate constant for

$$O^+ + O_2 \rightarrow O_2^+ + O \qquad (2)$$

are known. Over much of the height range of interest it is a good approximation to take the local electron and O^+ densities as equal, so the deduced densities for the ion may be compared to ionosonde or incoherent scatter measurements of electron densities wherever they are available. We shall show that in these cases the results of the two measurements agree very well when reasonable values are taken for the neutral densities and rate constants. In this way we can establish credibility for the airglow technique as a method for deducing electron (or ion) densities. Interestingly enough, the

airglow data usually pertain to the regions below the F_2 peak. Thus, the satellite observations constitute a form of topside sounding of the ionosphere below the F peak and provide synoptic data about this portion of the ionosphere otherwise impractical to obtain. For this type of sounding, the emission at 5577A is more suitable than the brighter emission at 6300A since $O(^1D)$ is strongly quenched in the lower F region whereas the $O(^1S)$ is not.

By appearing to require rather low values for the product of the O_2 density and the rate constant of reaction (2) to agree with ionosonde data, the airglow results also provide useful confirmation of conclusions arrived at as a result of other studies; namely, that the model densities of O_2 are too high and that the rate constant for reaction (2) decreases with ion temperature and is in the neighborhood of 5×10^{-12} cm^3 sec^{-1} at 1000°K.

Experiment

The photometer on OGO-6 (Experiment F26) is equipped with a mirror that is pivoted to scan the sky near the horizon. The scan extends below the horizontal plane of the spacecraft from about 10 to 25 degrees. The scan (requiring 18.43 seconds) is divided into 127 positions, each separated by 7.5 minutes of arc (the vertical field of view is also 7.5 minutes of arc, the horizontal field of view is 4.2 degrees). Thus, for the satellite at 500 km, the sampled emission feature at 250 km is less than 4 km high for a single mirror position. For a complete cycle, the photometer scans up and down with the green (5577A) filter, then up and down with the yellow (5890A) filter. Often the satellite is aligned with the photometer axis approximately in the orbital plane.

OGO-6 was launched in June, 1969, into a polar orbit inclined at 82° (apogee 1100 km - perigee 400 km). The orbital modes regress with a period of about 180 days, giving a very slowly changing local time for the observations.

Data Reduction

In Figure 1, a typical nightside pass is illustrated; the F-region green emission is usually seen only in the intertropical region. The F-region nightglow is first seen weakly at A, at mirror positions corresponding to slightly above 100 km. As the satellite moves to B, and then C, the emitting region appears to rise above the horizon and become more intense (the intensity increases since the slant path through the strong emission features increase). As the satellite moves to D and E, the region appears to set.

Figure 2 shows actual data that would correspond to similar circumstances. The 95 km nightglow clearly stands out. The F-region nightglow can clearly be seen to rise out of the low layer in the north. Figure 3 shows one scan in more detail; the photometer data, slant intensity, is plotted versus mirror position which is correlated with the altitude of the point on the optical axis that is closest to the center of the earth.

Since this emitting region is scanned from several (usually 20 to 30) positions, the shape, size, and volume emission rate can be determined. A general outline of the reduction procedure follows. All calculations are carried out in a spherically orthogonal coordinate system corresponding to the earth-centered magnet dipole approximation of the magnetic field. The emitting region is divided into areas 2 km

by 0.5 degrees (about 58 km) of magnetic dipole latitude. A volume emission rate is calculated for each area in the following manner. The boundary of the region is defined by setting to zero emission rates from areas that lie on optical axes which receive no signal. Then the emission rates are calculated by starting at the top, as most volumes of those optical axes contribute no emission. Using previously calculated volume emission rates, new emission rates are determined. When completed, the emission matrix (100 x 146) is smoothed with a running surface average of 10 km x 1.5 degrees. To improve this, each slant intensity that would be seen by the satellite is calculated and compared to the measured value, then elements of the emission matrix along that optical axis are rescaled accordingly (each is multiplied by the same factor). After the rescaling has been repeated twice for each measured intensity, the matrix is smoothed as above. The rescaling procedure is repeated five times. In this manner, volume emission rates consistent with measured data are generated. Along with the emission matrix, a matrix of residues (measured, less calculated slant intensity) is printed. The emission matrix is used to draw an emission contour map and to calculate electron densities.

There are several assumptions and approximations used in this procedure. The most significant source of error is misalignment of the photometer axis from the plane of the orbit. Data with large misalignments are not reduced. To correct for this, emission rates are projected onto the line of sight by assuming that the emission rate does not vary with longitude. For each line of sight, the height is calculated at 0.5 degree intervals of magnetic dipole latitude using spherical geometry in order to determine the corresponding emission matrix elements. Consider element A on this line of sight. It will also be on some lines of sight

for several other scans (i.e. a line of sight will pass through the same altitude and latitude simultaneously). However, on different scans this may be true at different longitudes. Equating these emission rates is exact when the satellite is precisely aligned. When the photometer is not looking in the orbital plane, the approximation may be poor if there are strong spatial variations in the ionosphere.

The following approximations are also used.

1. The time variation is small. The interval under consideration is about 10 minutes.

2. Both the vertical and horizontal fields of view are very small.

3. The satellite orientation and position are fixed during the entire scan (the error in satellite position is less than 0.5 degrees).

The emission map that results is consistent with the measured intensity (to within an error that is usually less than 10 percent), but it is not unique. Although details of the map change as data reduction procedure or input parameters are changed, the main features remain constant. Examples of these variables include the size of the smoothing interval, the manner in which dark current is calculated, and the mirror position calibration.

Observations

When the 5577A slant intensity records (for OGO-6 in eclipse) are examined, a strong signal from the 90-100 km region is always found in them. Near local midnight, except when auroras are encountered, the signal from F-region altitudes is almost entirely a tropical phenomenon. Occasionally small signals just above the noise are seen in the mid-latitude F-region. This places an upper limit of about a Rayleigh for the mid-latitude

F-region integrated vertical intensity. The 5577A emission maps on Figures 4-6, show that; the maximum emission rates lie between 225 and 300 km; the emission features are not symmetric about any equator; and the vertical integrated intensities are consistent with other observations. The contours are spaced logarithmically (each separated by a factor of 2) and show the exponential nature of the emission.

Calculation of Electron Densities

The important reaction for exciting the $O(^1S)$ is dissociative recombination (Reaction 1). The rate constant α_1 has been measured by Kasner and Biondi (1968) to be 2×10^{-7} $(300/T)$, when $T_e = T = T_+$ where T_e, T, and T_+ are the electron, neutral and positive ion temperatures. When $T = 300°K$, Mehr and Biondi (1969) found a temperature dependence of $(300/T_e)^{0.7}$ for $300° \leq T_e \leq 1200°K$. In the night time F-region, $T_e \approx T \approx T_+$ (McClure, 1969). The number k_s of $O(^1S)$ resulting from each dissociative recombination is about 0.1 (Zipf, 1970). The O_2^+ is produced by charge exchange (Reaction 2). The rate constant γ_1 is 2.0×10^{-11} $(300/T)^{0.5}$ (Ferguson, 1969). Because this reaction is much slower than (1), it controls the process.

To consider the complete ion picture, two more reactions must be included. NO^+ is produced by

$$O^+ + N_2 \rightarrow NO^+ + N \qquad \gamma_2 = 1.2 \times 10^{-12}(300/T)^{0.5} \qquad (3)$$

(Ferguson, 1969). Above 1000°K, the rate probably increases due to N_2 vibrational effect (O'Malley, 1970). The NO^+ produced may recombine,

$$NO^+ + e \rightarrow N + O \qquad \alpha_2 = 4.0 \times 10^{-7}(300/T) \qquad (4)$$

(Weller and Biondi, 1968), but not enough energy is availabel to excite $O(^1S)$.

Combining the reaction using the development of Peterson et al (1966), the volume emission rate is given by the relation

$$E = n^2 k(h)/(n + \gamma_1[O_2]/\alpha_1 + \gamma_2[N_2]/\alpha_2) \quad (5)$$

where

$$k(h) = .94\, k_s\, [O_2]\, \gamma_1 \quad . \quad (6)$$

Solving for the electron density n,

$$n = \frac{E}{2\, k(h)} \left\{ 1 + \left[1 + \frac{4\, k(h)}{E} \left(\frac{\gamma_1\, [O_2]}{\alpha_1} + \frac{\gamma_2\, [N_2]}{\alpha_2} \right) \right]^{1/2} \right\} . \quad (7)$$

Above 250 km $n \approx [O^+]$. Thus,

$$E = n\, k(h) \quad . \quad (8)$$

Comparison of Satellite and Ionosonde Data

By using equation (5), emission rates can be calculated from ionosonde data and thus compared to the emission rate inferred from the satellite data. Because of its equatorial location, Huancayo, Peru, ionosonde data was used (electron profiles were reduced by J. W. Wright's group, Boulder, Colo.). Coinciding data occurred on 2 November, 1969, at about 2330 hr. local time. Figure 7 shows that emission rate and electron density profiles are in good agreement. Since the shapes of the profiles are nearly the same, the only significant mechanism exciting the $O(^1S)$ must be dissociative recombination. The bump at 280 km is probably not significant as the electron density is smoothed over about 40 km when reduced and there is some uncertainty in the emission matrix.

To achieve the absolute agreement shown in Fig. 7, it is necessary to reduce, by a factor of 2.1, the value of the product shown in Equation (6). The use of k_s at 0.1, γ_1, as given above, and the O_2 densities of the Jacchia (1971) model atmosphere with T = 900°K produce a predicted rate 2.1 times too large at all altitudes. There is no way to decide which of these factors should be reduced from these observations alone. There is a strong indication from ion chemistry requirements in the ionosphere that at 900°K the value of γ_1 should be about 5.8×10^{-12} (Donahue, 1972) rather than 1.2×10^{-11} as calculated from the assumed rate. Using this lower rate, the agreement between the satellite and ionosonde 5577A intensities is within experimental error.

The above numbers depend on the absolute calibration of the photometer. An absolute calibration was performed before launch and relative gain changes are indicated by an on-board calibration system (using a tungsten lamp and performed at 5 minute intervals). To check the calibration, we compared the 5577A emission observed simultaneously from OGO-6 and Fritz Peak. The emission was entirely from the E-region. Assuming a uniform layer to deduce a vertical intensity from the satellite data we find a value 1.34 times as large as that measured from the ground at Fritz Peak. If we were to change our calibration to agree with Fritz Peak, we would be obliged to reduce further the product of O_2 density, charge exchange rate constant and efficiency of ^1S production. The most likely candidate would probably be the last quantity since laboratory measurements of k_s are unsatisfactory to about 25%. Furthermore, the values were obtained at 300°K; thus, reduction of k_2 to 7.5% from 10% is not impossible.

Electron Density Maps

The positive comparison of satellite-inferred and ionosonde data indicates that the emission maps may be converted to electron density maps (by equation 7). This now provides a satellite bottomside sounder for the intertropical region. Figure 4 shows emission and electron maps that correspond to data in Figures 2, 3, and 7. Some influence of the magnetic field on the ionosphere is indicated by the field lines (Figures 4-6). These are dipole field lines which were placed over the dip equator to better approximate the actual magnetic field near the surface. The N_e map indicates a strong drop in density at the upper edge. This is probably not real since very noisy and weak emission rates produced these values. The dashed lines on Figure 7 indicate the reliability of the electron densities deduced.

The ionospheric cross section shown in Figure 5 indicates a strong arc-like structure. Note that the lower northern arc gives a higher intensity while the electron densities are about the same, 10^6 electrons cm^{-3}. Since this reduction was made earlier, a model atmosphere from the U.S. Atmosphere Supplements 1966, with T_∞ = 1000°K, was used. Only a small change in shape would result as the magnitudes have been corrected. The data in Figures 4 and 5 are from November and are more variable than in Figure 6, which was from August (US 66 Atmosphere T = 900°K).

Results and Conclusions

Bottomside electron density maps in the intertropical region have been generated from OI 5577A data collected by a horizon scanning photometer on OGO-6. The contour maps show the variation of the electron

density and green emission; such maps have been previously impractical to obtain. A comparison of ground-based electron density measurement to the maps indicated that the emission results from dissociative recombination.

We also conclude that near 1,000°K the rate constant for O^+, O_2 charge exchange is smaller than the value obtained through the usually recommended extrapolation of laboratory measurements. This agrees with other ionospheric experience.

Acknowledgements

This work was supported by a grant from NASA, ~~NA5511077~~ NAS5-11077. We are indebted to the group at the Service d'Aeronomie under Professor J. E. Blamont who were largely responsible for the construction of the experimental equipment. Much of the early data reduction used in this work is due to Dr. Bruce Guenther who has contributed invaluable assistance and support. The entire OGO team is to be congratulated for their efficient handling of spacecraft operations and data analysis.

Finally, we would like to acknowledge the World Data Center and J. W. Wright's group of NOAA for electron densities profiles and G. Hernandez for vertical 5577A intensities from Fritz Peak.

References

Donahue, T. M., Positive ion chemistry of the D and E regions, Radio Science, to be published, 1972.

Ferguson, E. E., Laboratory measurements of F-region reaction rates, Ann. Geophys. 25, 819, 1969.

Gulledge, I. S., L. M. Packer, S. G. Tilford and J. T. Vanderslice, Intensity profiles of the 6300-A and 5577-A OI lines in the night airglow, J. Geophys. Res. 73, 5535, 1968.

Jacchia, L. G., Revised static models of the thermosphere and exosphere with empirical temperature profiles, Smithsonian Astrophysical Observatory Special Report 332, May 5, 1971.

Kasner, W. H., and M. A. Biondi, Temperature dependence of the electron -O_2^+ - ion recombination coefficient, Phys. Rev. 174, 139, 1968.

McClure, J. P., Diurnal variation of neutral and charged particle temperatures in the equatorial F-region, J. Geophys. Res. 74, 279, 1969.

Mehr, F. J., and M. A. Biondi, Electron temperature dependence of recombination of O_2^+ and N_2^+ ions with electrons, Phys. Rev. 181, 264, 1969.

O'Malley, T. F., Simple model for the high energy reaction of O^+ ions with N_2^*, J. Chem. Phys. 52, 3269, 1970.

Peterson, V. L., T. E. Van Zandt, and R. B. Norton, F-region nightglow emission of atomic oxygen, J. Geophys. Res. 71, 2255, 1966.

Van Zandt, T. E., and V. L. Peterson, Detailed maps of tropical 6300A nightglow enhancements and their implications on the ionosphere F_2 layer, Ann. Geophys. 24, 747, 1968.

Weller, C. S., and M. A. Biondi, Recombination, attachment, and ambipolar diffusion of electrons in photo-ionized NO afterglow, Phys. Rev. 172, 198, 1968.

Zipf, E. C., The dissociative recombination of O_2^+ ions into specifically identified final atomic states, Bull. Am. Phys. Soc. 15, 418, 1970.

Figure Captions

Figure 1 As the satellite views the F-region nightglow from positions A-E, the nightglow first appears to rise, then set. Since each small emission feature is viewed many times, it is possible to unfold the emitting region. The drawing is not to scale.

Figure 2 A series of scans for the green filter as the satellite moves across the equator.

Figure 3 An example of the photometer data when plotted versus apparent altitude, the altitude of the point on the optical axis closest to the center of the earth. The F-region intensity is unusually strong on this scan. The 100 km peak clearly shows the sharp fall off its top side.

Figure 4 This composite drawing shows information reduced from slant intensity data taken during a pass over the equator on 3 November, 1969. The upper map shows logarithmically spaced contours of the 5577A volume emission rate. By summing vertically, a vertical intensity was produced and is plotted in the center. By using the O_2 density and reaction rates each volume emission rate was transformed to an electron density; using these, the lower contour map was generated. Superimposed on the electron density map are magnetic field lines, these are generated from earth-centered dipole approximations but were centered over the dip equator. Due to misalignment of the photometer scan, it was necessary to assume that emission rates did not vary over about eight degrees of longitude.

Figure 5 Similar to Figure 4 but for 2 November, 1969. The longitude interval was about eight degrees.

Figure 6 Similar to Figure 4 but for 19 August, 1969. The longitude interval was about 15 degrees.

Figure 7 5577A emission rate from OGO-6 data (solid line) for the latitude of Hauncayo, Peru, and that inferred from Hauncayo ionosonde data (open circles). To match the curves, the OGO-6 data was moved up 15 km, and peak intensities were matched by varying k(h) (equation 6). Also, the reliability of electron density determined from emission rates is indicated.

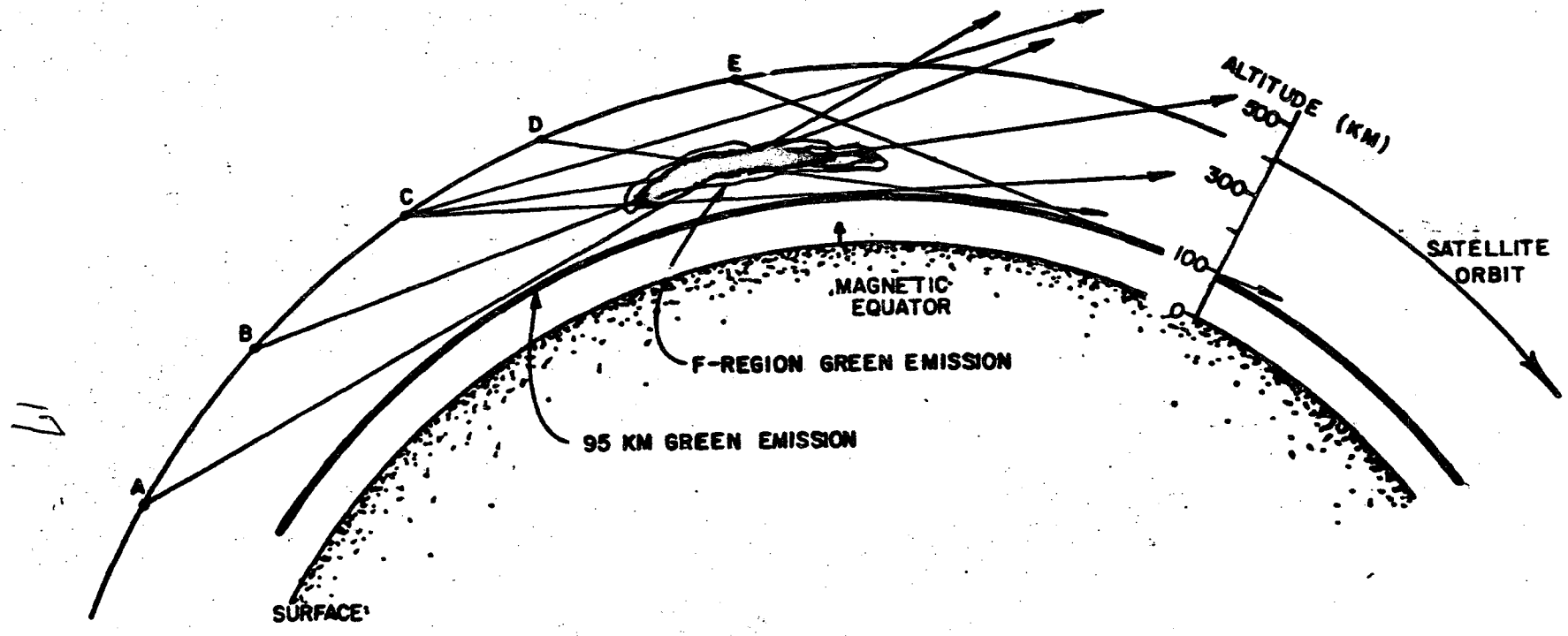
E
D
C
B
A
ALTITUDE (KM)
500
300
100
0
SATELLITE ORBIT
MAGNETIC EQUATOR
F-REGION GREEN EMISSION
95 KM GREEN EMISSION
SURFACE

Figure 1

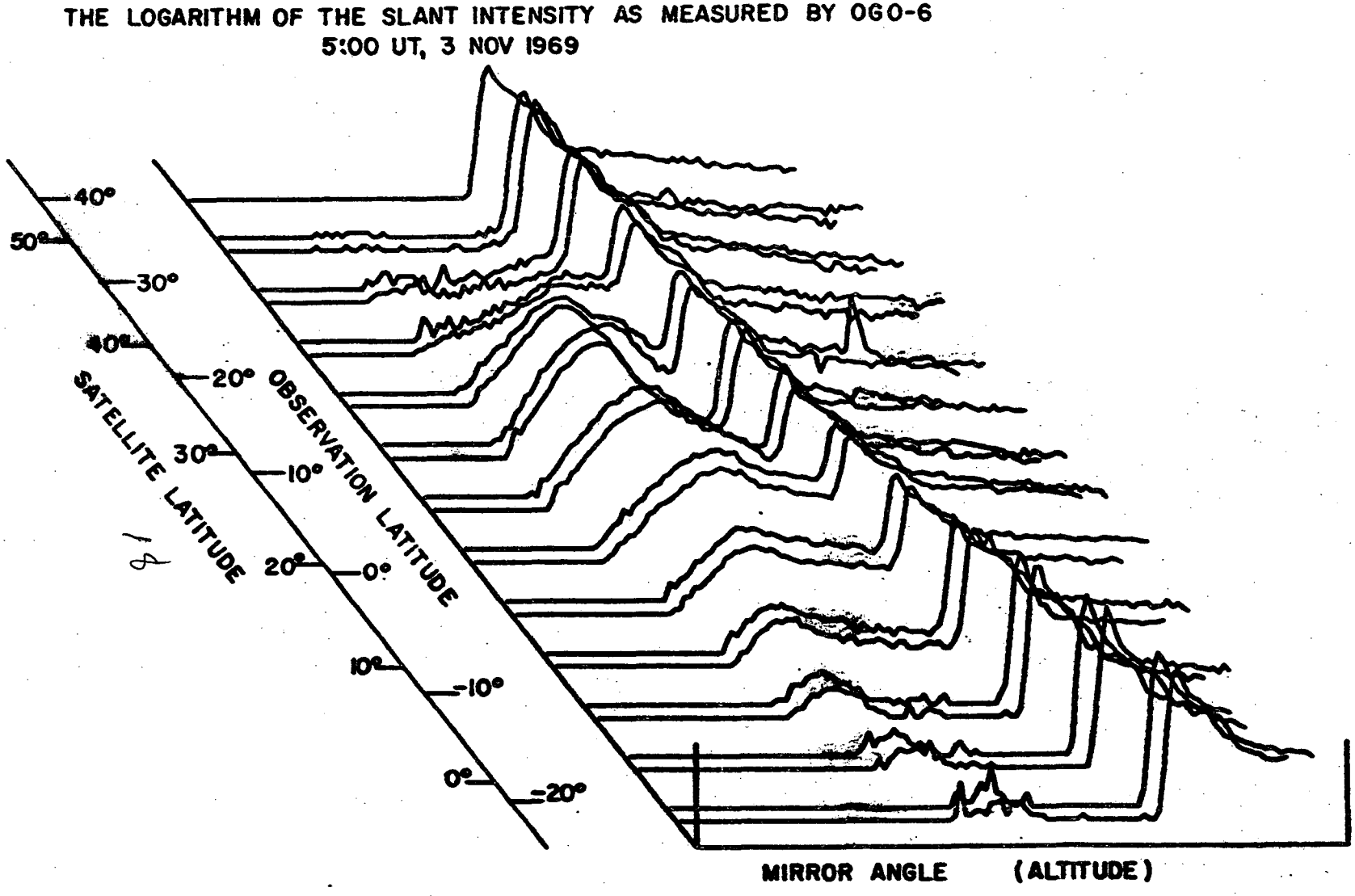
THE LOGARITHM OF THE SLANT INTENSITY AS MEASURED BY OGO-6
5:00 UT, 3 NOV 1969
40°
50°
30°
40°
20°
30°
10°
20°
0°
10°
-10°
0°
-20°
SATELLITE LATITUDE
OBSERVATION LATITUDE
MIRROR ANGLE (ALTITUDE)

Figure 2

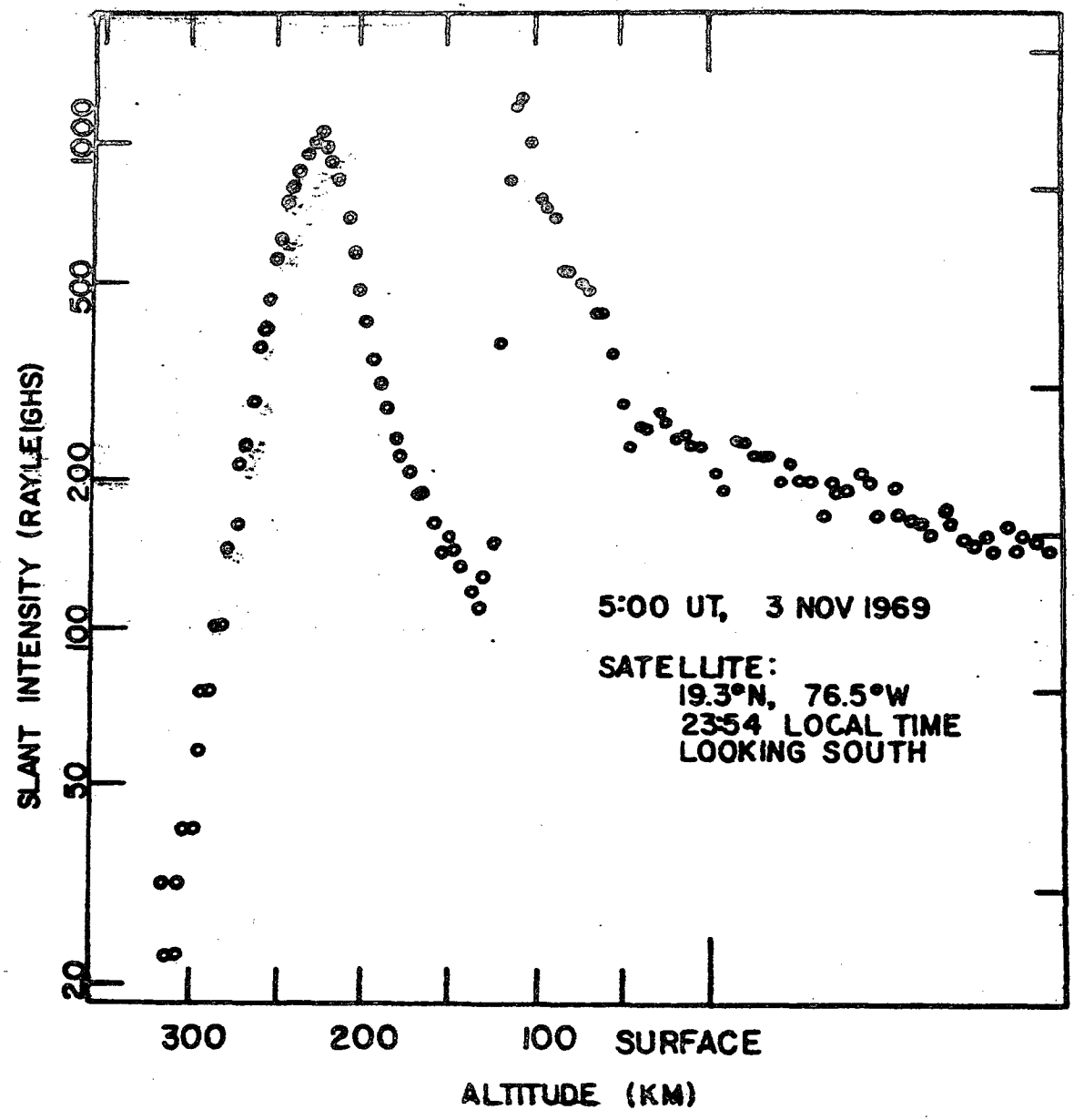
SLANT INTENSITY (RAYLEIGHS)
1000
500
200
100
50
20
5:00 UT, 3 NOV 1969
SATELLITE:
19.3°N, 76.5°W
23:54 LOCAL TIME
LOOKING SOUTH
300
200
100
SURFACE
ALTITUDE (KM)

Figure 3

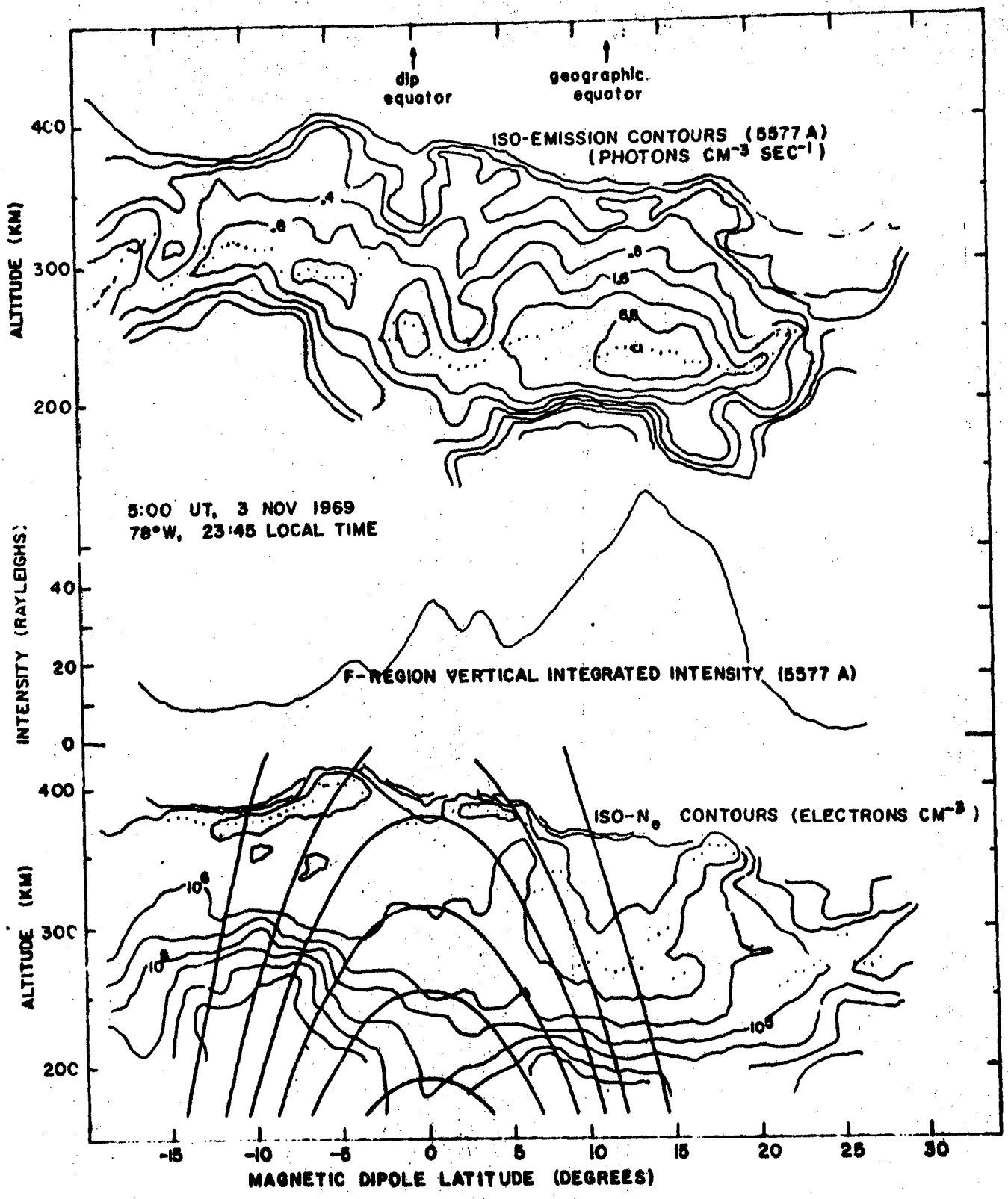
dip equator
geographic equator
ISO-EMISSION CONTOURS (6577 A)
(PHOTONS CM⁻³ SEC⁻¹)
ALTITUDE (KM)
400
300
200
.4
.8
.8
1.6
6.8
5:00 UT, 3 NOV 1969
78°W, 23:45 LOCAL TIME
INTENSITY (RAYLEIGHS)
40
20
0
F-REGION VERTICAL INTEGRATED INTENSITY (6577 A)
400
300
200
ISO-N_e CONTOURS (ELECTRONS CM⁻³)
10^6
10^5
10^5
-15
-10
-5
0
5
10
15
20
25
30
MAGNETIC DIPOLE LATITUDE (DEGREES)

Figure 4

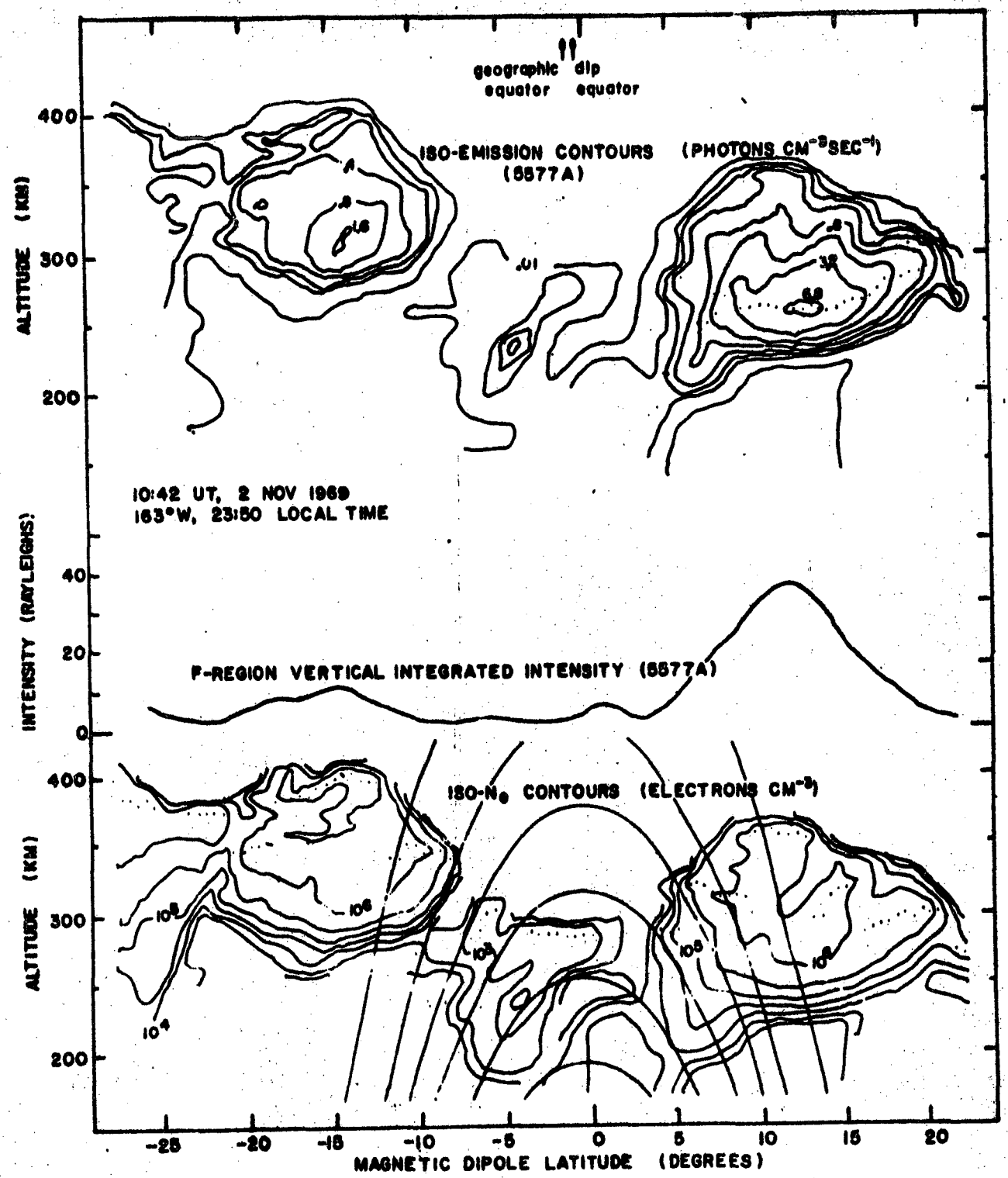
geographic equator
dip equator
ISO-EMISSION CONTOURS (PHOTONS CM⁻²SEC⁻¹)
(5577A)
ALTITUDE (KM)
400
300
200
10:42 UT, 2 NOV 1969
163°W, 23:50 LOCAL TIME
INTENSITY (RAYLEIGHS)
40
20
0
F-REGION VERTICAL INTEGRATED INTENSITY (5577A)
ISO-Ne CONTOURS (ELECTRONS CM⁻³)
10⁵
10⁴
-25
-20
-15
-10
-5
0
5
10
15
20
MAGNETIC DIPOLE LATITUDE (DEGREES)

Figure 5

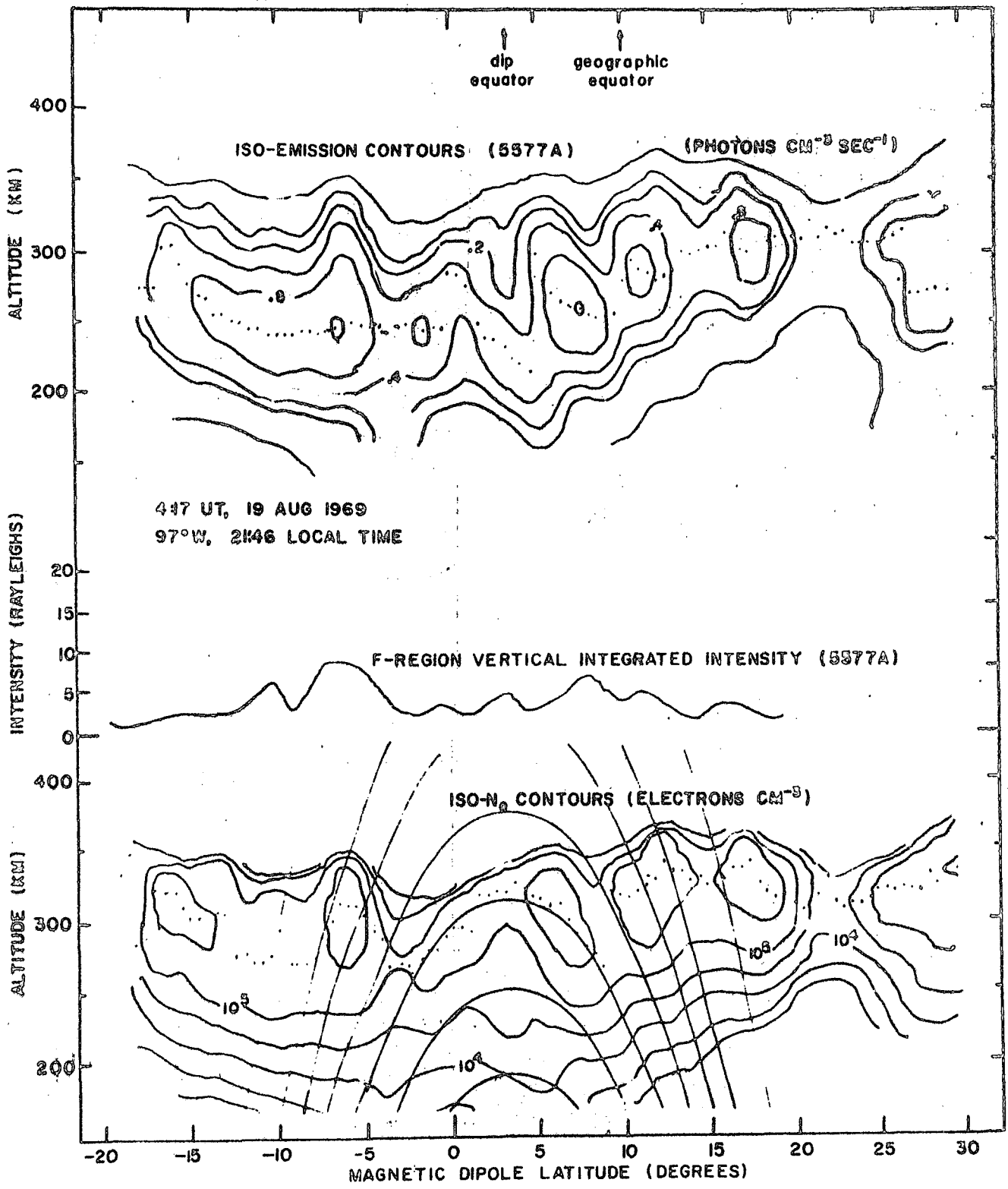
dip equator
geographic equator
ISO-EMISSION CONTOURS (5577A)
(PHOTONS CM⁻² SEC⁻¹)
ALTITUDE (KM)
400
300
200
.2
.4
.6
.8
4:17 UT, 19 AUG 1969
97°W, 21:46 LOCAL TIME
INTENSITY (RAYLEIGHS)
20
15
10
5
0
F-REGION VERTICAL INTEGRATED INTENSITY (5577A)
ISO-N_e CONTOURS (ELECTRONS CM⁻³)
10^3
10^4
10^5
10^6
-20
-15
-10
-5
0
5
10
15
20
25
30
MAGNETIC DIPOLE LATITUDE (DEGREES)

Figure 6

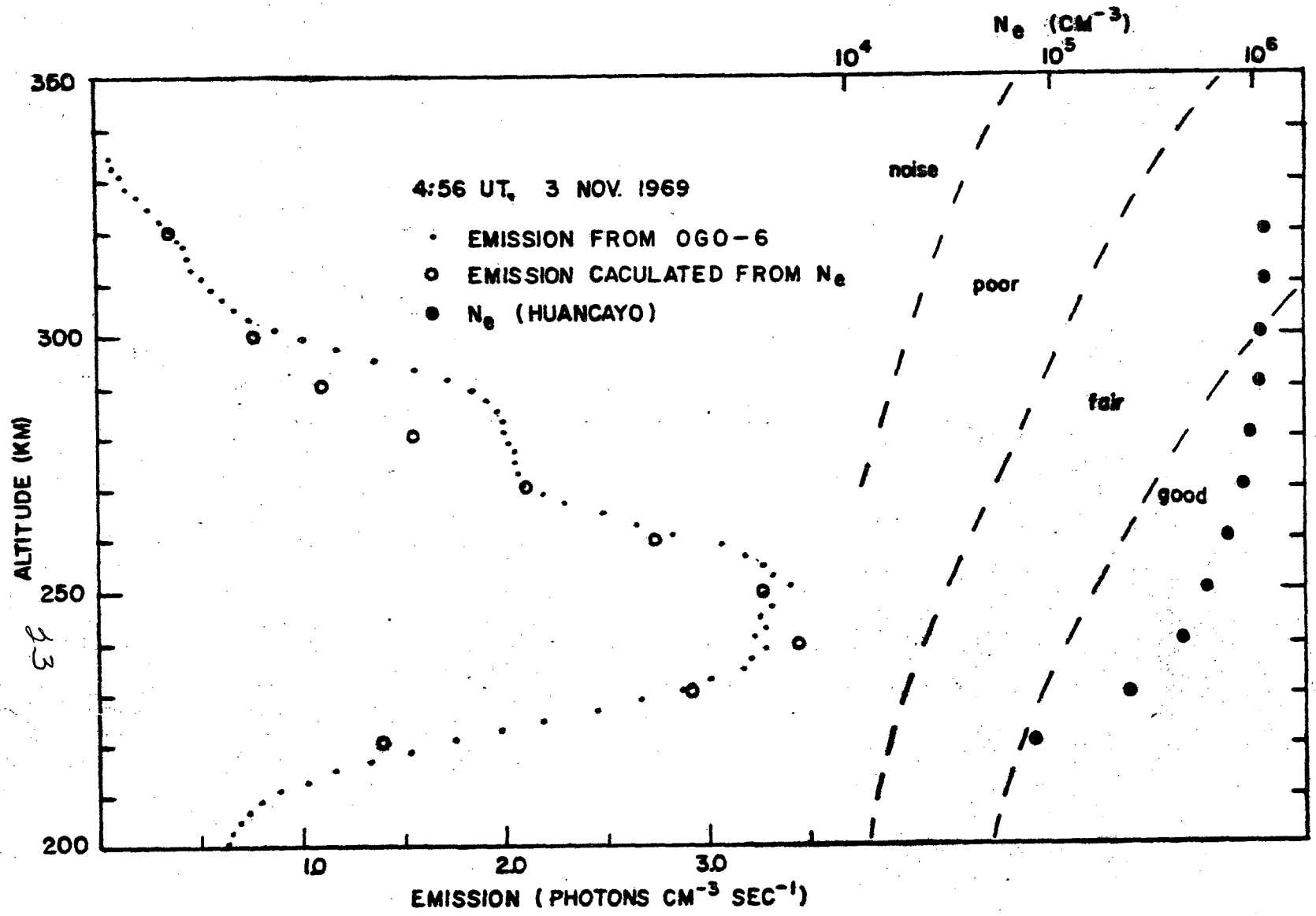
N_e (CM^{-3})
10^4
10^5
10^6
360
300
250
200
ALTITUDE (KM)
4:56 UT, 3 NOV. 1969
EMISSION FROM OGO-6
EMISSION CACULATED FROM N_e
N_e (HUANCAYO)
noise
poor
fair
good
1.0
2.0
3.0
EMISSION (PHOTONS CM^{-3} SEC^{-1})

Figure 7